Chemistry
A European
Journal

Chemistry Europe
European Chemical Societies Publishing

Accepted Article

Title: Bifunctional europium(III) and niobium(V)-containing Saponite Clays for the Simultaneous Optical Detection and Catalytic Oxidative Abatement of Blister Chemical Warfare Agents

Authors: Stefano Marchesi, Matteo Guidotti, Leonardo Marchese, Claudio Evangelisti, Fabio Carniato, and Chiara Bisio

To be cited as: *Chem. Eur. J.* 10.1002/chem.202005454

Link to VoR: https://doi.org/10.1002/chem.202005454

WILEY-VCH

10.1002/chem.202005454

RESEARCH ARTICLE

WILEY-VCH

Bifunctional europium(III) and niobium(V)-containing Saponite Clays for the Simultaneous Optical Detection and Catalytic Oxidative Abatement of Blister Chemical Warfare Agents

Stefano Marchesi,[a] Matteo Guidotti,[b] Leonardo Marchese,[a] Claudio Evangelisti,[c] Fabio Carniato,*[a] and Chiara Bisio*[a,b]

[a] Dr. S. Marchesi, Prof. L. Marchese, Prof. F. Carniato, Prof. C. Bisio
Dipartimento di Scienze e Innovazione Tecnologica
Università del Piemonte Orientale *"Amedeo Avogadro"*
Viale Teresa Michel 11, 15121-Alessandria, Italy
E-mail: fabio.carniato@uniupo.it; chiara.bisio@uniupo.it

[b] Dr. M. Guidotti, Prof. C. Bisio
CNR-SCITEC - Istituto di Scienze e Tecnologie Chimiche *"G. Natta"*, Milano
Via C. Golgi 19, 20133-Milano, Italy

[c] CNR-ICCOM Istituto di Chimica dei Composti Organo Metallici, via G. Moruzzi 1, 56124 Pisa, Italy

Supporting information for this article is given via a link at the end of the document.

Abstract: For the first time, the co-presence in the saponite structure of luminescent Eu(III) and catalytic Nb(V) metal sites was exploited for the simultaneous detection and catalytic abatement of sulfur-containing blister chemical warfare agents. Metal centres were introduced in structural positions of the saponite (in the interlayer space or inside the inorganic framework) following two different synthetic methodologies. The functionalized saponites were able to reveal the presence of a sulfur mustard simulant (2-chloroethyl)ethyl sulfide (CEES) after few seconds of contact time and more than 80% of the substrate was catalytically decomposed after 24 h in the presence of aqueous hydrogen peroxide.

Introduction

Different types of chemical warfare agents, CWA, have been developed and employed in warfare scenarios and in terroristic attacks worldwide.[1-5] Sulfur- and nitrogen-containing blister agents (*i.e.* sulfur mustard or yperite), incapacitating agents (*i.e.* tear gases, fentanyl) and organophosphorus nerve agents (*i.e.* sarin, VX) have attracted the widest attention along the last 100 years.[6-9] Because of their high toxicity to living organisms and environment, and due to the current delicate global geopolitical situation,[6,7] CWAs are still a threat for humankind.

It is thus essential to develop efficient and sustainable procedures for a correct and safe destruction or abatement of CWAs.[10,11] At the same time, a timely detection of highly toxic agents can promptly reveal the presence (or the absence) of immediate health risks to operators who have to deal with these extremely hazardous materials.[12-15] Designing and obtaining materials with a combined detection/decontamination capability would be a remarkable added value. However, reports of smart solids displaying both properties at once have been presented only marginally, so far. In these cases, polyoxometalates were able to reveal the presence of blister agents by colour changes and catalytically degrade them, although in the presence of complex and scarcely sustainable co-reactants.[14] Likewise, supramolecular diamide organogels showed sensing and decontamination properties, but stoichiometric amounts of tetrabutylammonium 4-benzaldoximate, as a reactive decontaminant, were necessary to carry out the detoxification of the organophosphorus compound.[13] Carbon-supported ytterbium molybdate nanoflakes need a light source to complete the photocatalytic abatement of the nerve CWA simulant.[15]

Currently, conventional decontamination procedures are based on: *i*) physical removal by adsorption of CWAs on the surface of different solids or dissolution in organic solvents; *ii*) thermal elimination at high temperatures; *iii*) use of advanced techniques based on microwaves and plasma treatments; *iv*) over-stoichiometric oxidation reaction with active chlorine-based oxidants.[16,17]

These methods are quite efficient, but they suffer from important drawbacks in terms of costs and environmental impact. Indeed, they typically require large amounts of reactants, high energy and equipment costs.[10,11,18]

To overcome these limits, heterogeneous nanostructured solid catalysts proved to be excellent systems for the selective oxidation of CWAs into partially or fully oxidized non-toxic products.[19-21] Transition metals-polyoxometalates containing V, Mo and Fe,[22,23] porous oxides decorated with different metal sites,[16,24,25] metal-containing silica or zeolite, metal organic frameworks (MOFs) and modified activated carbons were explored in this field with encouraging results for the CWAs degradation.[19,20,26-29]

Recently, synthetic saponite clays[30] and natural montmorillonites functionalized with Fe^{3+} ions,[31] attracted great interest thanks to their high robustness, chemical versatility, enhanced adsorption capabilities and low production costs.[32] In particular, a synthetic saponite featuring Brønsted acidity and catalytically-active Nb(V) is able to promote the oxidative decontamination of more than 90% of (2-chloroethyl)ethyl sulfide, CEES, into non-noxious products in few hours, under very mild conditions in *n*-heptane with diluted hydrogen peroxide as oxidant.[30]

On the other hand, as far as detection methods based chemosensors are concerned,[33-40] luminescent lanthanides (*i.e.* Eu(III), Tb(III), Er(III)), alone or in combination with other transition metals ions,[41-43] have been recently proposed as ideal candidates for the development of novel optical sensing platforms.[44] In particular, Eu(III) shows unique spectroscopic characteristics, including long fluorescence lifetime, high quantum efficiency, large Stoke shift (with excitation in the ultraviolet region and emission in the UV-Visible range) and narrow and intense emission bands, which are highly sensitive to even slightly changes in the chemical surroundings.[45]
In order to combine both detection and catalytic CWA degradation capabilities into a single nanostructured, robust and viable material, two synthetic saponites containing Eu(III) and Nb(V) sites were designed, prepared and tested in mild conditions (r.t., neutral pH and ambient pressure, aqueous medium) for this dual application, within this work.

Results and Discussion

Characterization of Eu(III)/Nb(V)-loaded saponites

Two solids containing Eu(III) and Nb(V) sites located in different positions, either inside the inorganic framework or in the interlayer region of saponite synthetic clay, were synthesized. The first sample (hereafter named NbEuSAP) was prepared by adapting the conventional hydrothermal *one-pot* approach followed for the saponite synthesis.[30,46] Both Eu(III) and Nb(V) precursors were simultaneously introduced into the clay synthesis gel during the synthetic procedure, to ensure the inclusion of the metal ions in the inorganic framework in a single step, without further modifications of the final material named NbEuSAP (Figure 1, C; Scheme S1). The second solid (Eu-NbSAP) contains the Nb(V) and Eu(III) sites in two different structural positions. It was prepared following three consecutive synthetic steps (Scheme S2): *1*) Nb(V) was introduced in the tetrahedral layer of clay using a *one-pot* hydrothermal method,[30] thus obtaining the NbSAP sample (which was also used as reference) (Figure 1, A); *2*) NbSAP clay was submitted to a first ionic exchange procedure in NaCl solution in order to promote the complete substitution of the interlayer ions (H^+, Al^{3+}, Mg^{2+}) by Na^+; *3*) Na-NbSAP was then treated with an aqueous solution containing $EuCl_3$ at acid pH (*ca.* 4), favouring a partial replacement of the intercalated Na^+ ions by Eu^{3+} (Figure 1, B).
It is important to note that the confinement of Nb(V) centres in the crystal lattice for both samples is extremely important for the catalytic performance. Following this strategy, the metal sites are chemically stabilized being less leachable during the catalytic test in aqueous solution.[30]

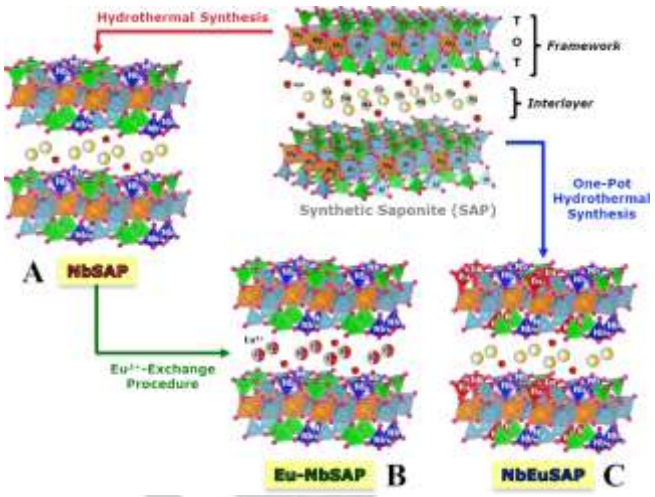

Figure 1. Synthetic pathways adopted for the preparation of reference NbSAP (A), Eu-NbSAP (B) and NbEuSAP (C) clays.

The Nb(V) and Eu(III) content in prepared samples was determined by inductively coupled plasma atomic emission spectroscopy (ICP-AES) after mineralization of the solids in acidic media (Table 1). Eu-NbSAP showed an amount of structural Nb(V) and intercalated Eu(III) equal to 0.18 and 0.30 mmol/g, respectively. Nb(V) content remained essentially unchanged after sodium- and europium-exchange, suggesting that the niobium metal centres are firmly located in the lattice sites of the saponite structure.[30] The *one-pot* NbEuSAP sample, instead, contains a lower amount of both Eu(III) (0.03 mmol/g) and Nb(V) (0.02 mmol/g) species. Such a difference, when compared to the previous sample, is likely due to the fact that when silicon, aluminium, niobium and europium ions are contemporarily present in the synthesis gel ions, the first two elements are more favourably accommodated in the tetrahedral layer.

Table 1. Nb(V) and Eu(III) loading for NbSAP, Eu-NbSAP and NbEuSAP.

Sample	Nb(V) [mmol/g]	Eu(III) [mmol/g]
NbSAP	0.19 ± 1.98E-3	/
Eu-NbSAP	0.18 ± 1.70E-3	0.30 ± 2.05E-3
NbEuSAP	0.02 ± 1.57E-3	0.03 ± 1.65E-3

Cationic exchange capacity (CEC) evaluated by UV-Vis spectroscopy,[47] resulted 45.5 ± 4.3 meq/100 g and 59.9 ± 5.1 meq/100 g for Eu-NbSAP and NbEuSAP, respectively. These values are comparable with the ones reported for previous Nb(V)-containing saponites.[30] X-ray powder diffraction (XRPD) analysis showed that in all cases, the presence in the structure of niobium and europium ions did not influence the crystallographic structure of saponite (Figure 2).[30,48] This is proved by the presence of the (001), (110)-(020), (004), (130)-(201), (311) and (060) reflections typical of saponite materials (Fig. 2a)[46] in both Eu-NbSAP (Fig. 2c) and NbEuSAP (Fig. 2d) clays. These results confirm the success of the synthetic procedures used for the preparation of these unprecedented

metal-functionalized clays. The basal plane (001) of NbEuSAP is more defined respect to the other samples, indicating an improved packing order of the lamellae.[46] The introduction of Eu^{3+} ions in the interlayer space of Eu-NbSAP (by means of ion exchange procedure), promoted a shift of the basal plane (001) of the saponite (Figure 2). The d(001) spacings were measured with greater accuracy by fast-Fourier-transform (FFT) of HRTEM selected areas (*vide infra*). The increasing of the (001) basal plane is correlated to the incorporation of the Eu^{3+} in the interlamellar region of the NbSAP sample and can be attributed to the larger hydration sphere of the Eu^{3+} ions.[47]

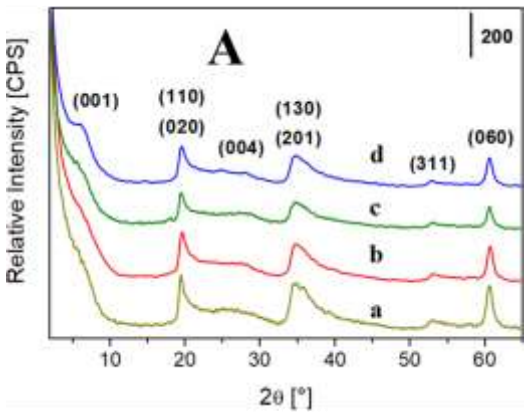

Figure 2. A) X-ray profiles of SAP-20 (a), NbSAP (b), Eu-NbSAP (c) and NbEuSAP (d).

The morphological features of reference NbSAP and Eu-NbSAP and NbEuSAP were evaluated by high-resolution transmission electron microscopy (HRTEM) (Figure 3A-C). The materials showed different levels of spatial organization of lamellae particles (*i.e.* from sheet-like single structures to tactoids of different size), with a range of lengths of a few tens of nanometres. The distribution of the $d_{(001)}$-spacing values, obtained by measuring at least 50 spots in the FFT patterns for each sample collected in micrographs acquired at different magnifications (Figure S1), was inhomogeneous and centred around 1.2-1.4 nm (Figure 3). The saponite interlayer space of Eu-NbSAP resulted increased of *ca.* 0.1 nm, with respect to the other samples.

Both, Eu-NbSAP and NbEuSAP solids displayed comparable textural features, investigated by N_2 physisorption at 77 K, with type IV isotherms typical of micro- and meso-porosity and with an H3 hysteresis loop, indicative of the presence of disordered aggregates (Figure S2). Similar textural properties were already observed for saponites prepared with high H_2O:Si ratio used in the gel synthesis.[46,49] The specific surface area (SSA) was found to be 332 and 312 $m^2\ g^{-1}$ for Eu-NbSAP and NbEuSAP, respectively, as estimated by the Brunauer-Emmett-Teller (BET) equation. Both materials also showed similar pore distributions, with maximum values centred at 53 Å. The pore volume resulted to be 0.453 $cm^3\ g^{-1}$ for Eu-NbSAP and 0.408 $cm^3\ g^{-1}$ for NbEuSAP solid.

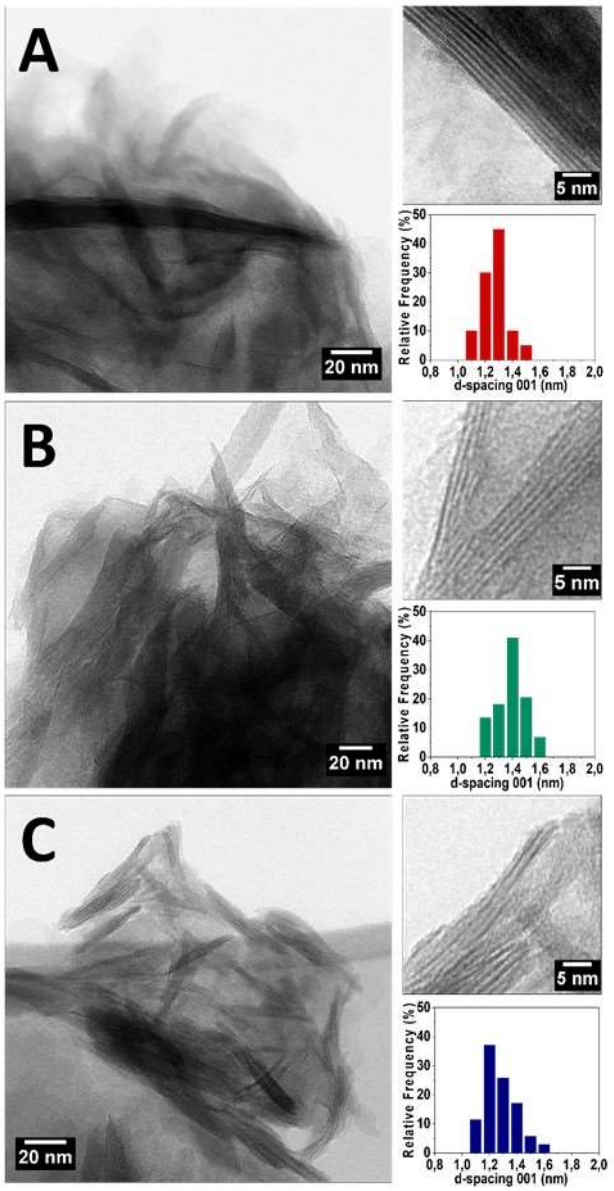

Figure 3. HRTEM micrographs and histogram of d(001)-spacing distribution of NbSAP (A), Eu-NbSAP (B) and NbEuSAP(C).

The coordination state of the Nb(V) species in NbSAP, Eu-NbSAP and NbEuSAP samples was investigated by Diffuse Reflectance UV-Vis spectroscopy (DR UV-Vis, Figure 4). The spectra showed two main absorptions: the most intense at 235-250 nm is assigned to charge-transfer (CT) transitions between oxygen atoms and Nb(V) in tetrahedral coordination, while the second one, at 270 nm, mainly evident for NbSAP and Eu-NbSAP samples containing higher Nb(V) loading, is attributed to structural octahedral Nb(V) species of the lamellae.[21,30] The less intense band at 320 nm is commonly associated to the presence of Nb(V) oxidic oligomers.[30] Such band is nearly absent in NbEuSAP sample (Figure 4, c) because of the lower Nb(V) loading in this solid. In all spectra, in general, no absorption bands were detected above 400 nm, thus suggesting the absence of large extra-phase Nb_2O_5-like domains.

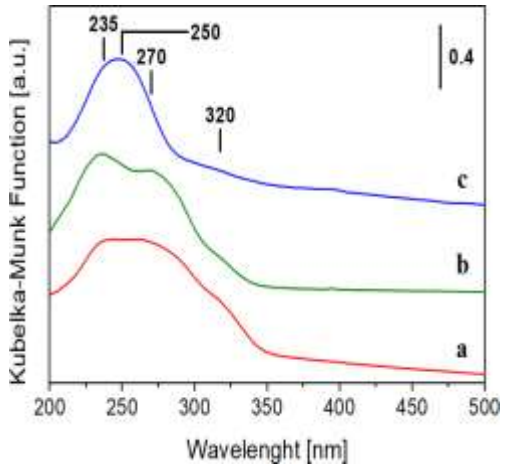

Figure 4. Normalized DR UV-Vis spectra of NbSAP (a), Eu-NbSAP (b) and NbEuSAP (c), diluted in $BaSO_4$ matrix (20 wt.%), in air and at RT.

The quantification of acid sites in the samples was performed by using FTIR spectroscopy of adsorbed ammonia.[50] Figure S3 shows the FTIR spectra collected after admission of 95 mbar of NH_3 at RT on the three samples and subsequent evacuation a RT for 90 min. The concentration of Brønsted acid sites was determined by considering the FTIR band of NH_4^+ at 1445 cm^{-1}.[46] The total concentration of Brønsted acid sites is comparable for all the samples, with values of 0.08, 0.09 and 0.11 mmol/g for NbSAP, Eu-NbSAP and NbEuSAP, respectively.

The photophysical properties of Eu(III)-containing clays were studied by photoluminescence (PL) spectroscopy, both in powder and in aqueous suspensions to obtain information on the chemical nature of the environment around Eu(III) sites. The aqueous suspensions were prepared by introducing few milligrams of solid in water in the presence of 0.1 wt.% of xanthan gum suspending agent.[51-52] The excitation spectrum of NbEuSAP (Figure 5A), recorded at the most intense emission line of Eu(III) at 615 nm, presented the narrow peaks due to the characteristic intra-4f^6 electronic transitions of Eu^{3+} ($^7F_{0,1}$-$^5D_{4\text{-}3}$, $^7F_0$-$^5D_2$, $^7F_0$-^5G_J, $^7F_0$-$^5L_{10\text{-}6}$) with the most intense excitation band at 395 nm due to $^7F_0$-$^5L_6$. The same bands were found for the Eu-NbSAP sample. The emission spectra of both luminescent clays were collected under irradiation at 395 nm (λ_{max} of Eu^{3+}) and showed the typical emission peaks of the intra-4f^6 electronic levels of Eu^{3+} ($^5D_0$-^7F_J, J = 0-4) (Figure 5B).[45] Similar results were obtained for the samples in the form of powder packed into the quartz cell (Figure S4). Additional photophysical information on heterogeneity of Eu^{3+} sites,[53] geometrical/coordination of Eu^{3+} centres (asymmetry/symmetry of the local environment),[54-57] hydration state,[54,57] quantum efficiencies[58,59] and photostability of the samples were also thoroughly studied by PL spectroscopy (Figure S4-7), and the results summarized in Table S1. For both materials, the local environments surrounding the luminescent centres were found to be highly asymmetric, with a variable amount of water molecules coordinated to Eu(III) for NbEuSAP and Eu-NbSAP, respectively. The average hydration of the Eu^{3+} ion (q) was estimated by the analysis of the photoluminescence lifetimes (τ) of the solids both dispersed in water and in D_2O. The decay curve of the $^5D_0$ level was fitted by applying the equation reported in literature.[54] The number of coordinated water molecules estimated for NbEuSAP was ca. 3 (Table S1).

An expansion of the hydration sphere for the intercalated Eu^{3+} in Eu-NbSAP with a q value between 4 and 5 was then determined.

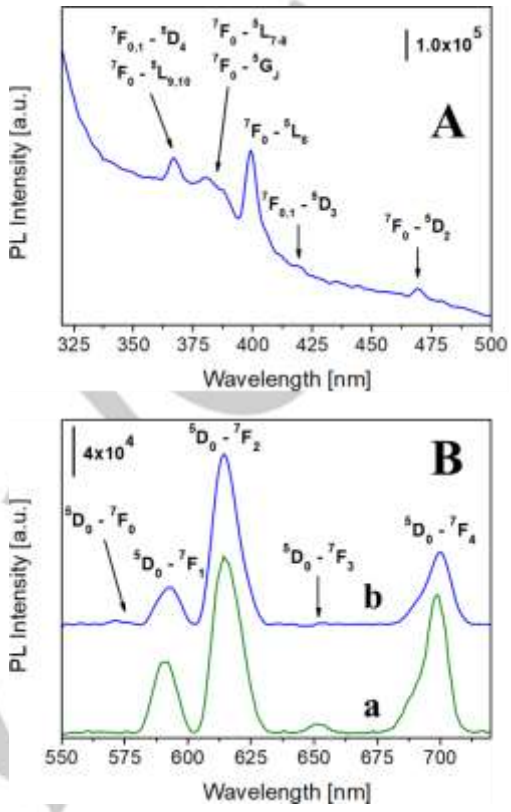

Figure 5. A) Excitation spectrum of NbEuSAP, collected at 615 nm. B) Emission spectra of Eu-NbSAP (a) and NbEuSAP (b), under excitation at 395 nm (λ_{max} Eu^{3+}). The spectra were collected in aqueous suspensions (with 0.1 wt.% of xanthan gum).

The stability of the aqueous suspensions of the prepared materials was evaluated by dynamic light scattering (DLS) analyses, whose measurements were performed at 25 °C. The suspensions of the samples remained qualitatively homogenous and stable for *ca*. 20 h, showing hydrodynamic diameters of the particles in the 45-70 nm nanometre range (Figure S8), with PDI distributions in the 0.55-0.85 nm range associated to the presence of particles with different size.

Catalytic Oxidative Abatement Tests

The catalytic oxidative abatement capability was tested in aqueous suspensions of the blister agent simulant CEES. The experiments were carried out under very mild conditions, *i.e*., at neutral pH (in phosphate buffer solution, PBS), room temperature and under atmospheric pressure, in the presence of diluted H_2O_2. More details on the experimental procedure are reported in the supporting information file. An experiment without catalyst (*blank*) was performed in order to assess the stability of CEES in water (Figure S9A). A pristine SAP-20 clay as reference (Nb-free) sample was also tested as catalyst for CEES degradation (Figure S9B).

The gradual consumption of CEES by Nb(V)-containing catalysts over time was followed by UV-Vis spectroscopy (Figures 6, S9C and S9D), by monitoring the decrease of the

absorbance of the main band of CEES at 200 nm, ascribed to $n \rightarrow \sigma^*$ electronic transitions of the molecule.[60]

Eu-NbSAP and NbSAP showed the same behaviour (Figure S9C and D, respectively). A negligible non-catalysed CEES self-decomposition (*ca.* 2 % after 24 h) is promoted by a weak oxidant activity of H_2O_2. CEES conversion of 29% is observed after 24h in the presence of pure SAP-20, thus proving that the clay itself is able to promote a partial degradation of the substrate because of its intrinsic Brønsted acidity (0.09 mmol/g) (Figure 6B, *d*).[30] A similar behaviour was previously observed when the catalytic test was carried out in *n*-heptane.

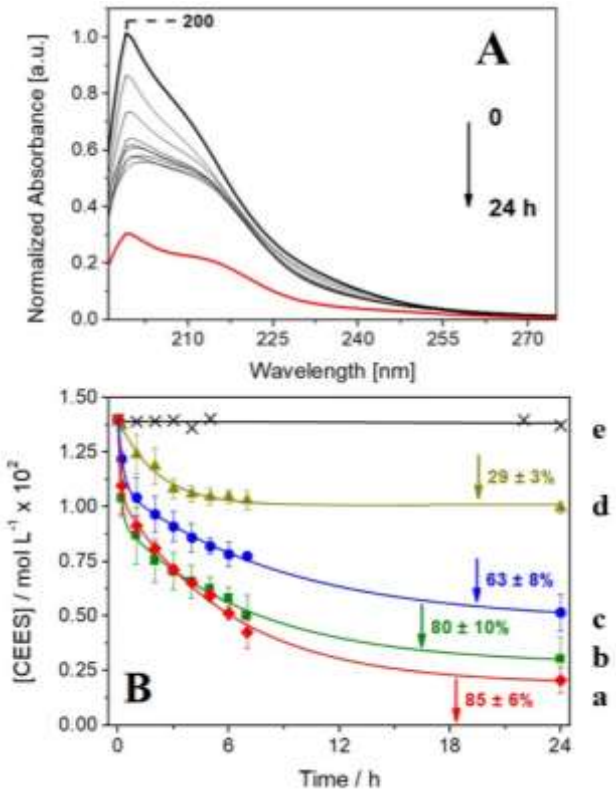

Figure 6. A) UV-Vis spectra of the reaction mixture in the presence of NbEuSAP catalyst, from 0-24 h. B) Oxidative abatement of CEES in the presence of NbSAP (a, -♦-), Eu-NbSAP (b, -■-), NbEuSAP (c, -●-), SAP-20 (d, -▲-) and without catalyst (e, -X-). Reaction conditions: 14 mM CEES, 70 mM 30 % aq. H_2O_2, PBS solution at neutral pH, 20 mg of catalyst and 25 °C.

The synergistic effect between Nb(V) centres and acid sites, which was previously evidenced by comparing the performance of proton-containing and proton-free Nb-saponites[30], was observed in these systems too: Nb(V) centres confer oxidizing properties, while the presence of Brønsted acid sites help to increase the abatement activity via an acid-promoted degradation. Furthermore, H^+ sites take part in the formation of niobium hydroperoxo-species, in which the selective heterolytic O_2 transfer from H_2O_2 to CEES takes place.[61,62] NbSAP (a) and Eu-NbSAP (b) samples presented the best catalytic performance, with more than 80 % of CEES decomposition after 24 h. NbEuSAP sample (c), containing both Nb(V) and Eu(III) ions in the structural positions of saponite, showed a slightly lower catalytic activity, *i.e.* about 63 %.

The synergistic effect between Nb(V) centres and acid sites H^+ in the formation of niobium peroxo species was further proved by analysing the interaction of the Nb-containing solids with an appropriate amount of 30 wt.% H_2O_2, through DR-UV-Visible spectroscopy, following a procedure optimized in the literature.[63] Figure S10 describes the experiment performed on the Eu-NbSAP (used as an example) and shows the UV-Vis spectra of the solid catalyst before and after the test. The spectrum of the sample treated with H_2O_2 shows new absorptions at 253 nm (with a shoulder at 230 nm) associated only to CT transitions oxygen to Nb(V) in tetrahedral coordination in comparison to the original bands at 235 and 270 nm related to Nb(V) sites. Most importantly, a new signal at 292 nm appears, fairly resolved with respect to the absorption tail of the starting material, which can be assigned to protonated peroxo-Nb(V) species Nb(V)(η^2-O_2), as described in the literature.[63] However, due the complexity of the spectroscopic features of these layered materials, we cannot completely exclude the presence also of hydroperoxo units.

The different catalytic behaviour has to be attributed to the concentration of Nb(V) sites because all solids have comparable amount of acid sites. Indeed, NbSAP and Eu-NbSAP with the best performance have a niobium loading *ca.* 10 times higher than the NbEuSAP sample. Moreover, the absence of niobium oxide domains in all samples allows to exclude any effect of these species on the final catalytic behaviour of the solids.[64]

In none of the tests, H_2O_2 was the limiting agent for the reaction. Actually, residual H_2O_2 were always detected at the end of 24 h. Oxidant efficiency values were in the range of 50-58%, for Nb-containing catalysts (Figure S11).

In all Nb-containing saponites a gradual loss of the catalytic activity after the first hours of reaction was observed. The main reason can be attributed to a gradual deposition of heavy organic deposits on the surface of the catalysts, hence hampering the catalytic activity. The presence of such deposits was evidenced by C,H,N elemental analysis and thermogravimetric measurements. In fact, percentages of organic deposits as high as 3.5 – 5.0 % were observed at the end of 24 h reaction, after a thorough washing and abundant rinsing with ultrapure water (see, for instance, Figure S16). A very different behaviour, with a far lower occurrence of organic deposits and catalyst deactivation was observed when NbSAP catalysts were tested in CEES oxidative degradation in *n*-heptane as a solvent.[30] In this last case, the apolar hydrocarbon solvent was partially able to remove the deposit and mitigate the deactivation process.

CEES decomposition was also monitored by high resolution ^{1}H-NMR to determine the chemical nature of the reaction products (Figures S12-14). A comparison of the NMR spectra of CEES alone (a) and in the presence of NbSAP (b), Eu-NbSAP (c) and NbEuSAP (d) catalysts after 5 h of contact time is reported in Figure S15.

The ^{1}H-NMR spectrum of CEES alone (Figure S12) shows the four characteristic peaks of the CWA simulant at chemical shift of 1.30 (triplet/*t*, -C*H*$_3$,), 2.58 (quartet/*q*, S-C*H*$_2$), 2.77 (*t*, C*H*$_2$-S) and 3.75 ppm (*t*, Cl-C*H*$_2$).[22] With no catalyst, CEES is stable over time in water, confirming previous UV-Vis observations.

Over Nb(V)-containing samples, CEES is hydrolysed, chlorine is lost and hydroxyethyl ethyl sulfide is formed after 5 h of reaction (Figure S15).[65,66] In the presence of NbSAP an almost complete disappearance of the signals of CEES is found (Figure S15). The ^{1}H NMR spectra for the solutions treated with Eu-NbSAP

(Figure S15c) and NbEuSAP (Figure S15d) samples, instead, showed only two weak signals at 2.58 and 2.77 ppm, assigned to C*H*$_2$ groups around the central sulfur atom in the CEES structure. In all cases, four main degradation products were clearly detected: (2-chloroethyl)ethyl sulfoxide (CEESO) and (2-chloroethyl)ethyl sulfone (CEESO$_2$), along with (2-hydroxyethyl)ethyl sulfoxide and (2-hydroxyethyl)ethyl sulfone (Figure S15).[22] The overoxidation of chlorosulfide and cholorosulfoxide led to the chlorosulfone CEESO$_2$, that is almost as toxic as the pristine substrate. However, thanks to the aqueous medium where the reaction is carried out, a large percentage of oxidised products were indeed hydroxy-sulfoxide and hydroxy-sulfone (namely, 2-(ethylsulfinyl)ethanol and 2-(ethylsulfonyl)ethanol), which are due to hydrolysis of the parent chlorocompounds and whose toxicity is far lower than the one of chloroderivates.[67] The selectivity to chloroderivates (CEESO, CEESO$_2$) and hydroxyderivates (OH-EESO, OH-EESO$_2$) at various reaction times can be extracted by merging the evidences from GC-MS and ^{1}H-NMR spectra (Table 2).

Table 2. Selectivity values to to chloroderivates and hydroxyderivates vs. time over Nb-containing catalysts.

Catalyst	Sel[a] (%) 1 h			Sel (%) 5 h			Sel (%) 24 h		
	OH	CEESO	CEESO$_2$	OH	CEESO	CEESO$_2$	OH	CEESO	CEESO$_2$
NbSAP	40	28	32	38	23	39	32	14	53
Eu-NbSAP	61	17	21	52	23	25	51	13	36
NbEuSAP	68	13	19	60	19	21	57	10	33

a: selectivity (%) to products. OH: sum of hydroxyderivates OH-EESO + OH-EESO$_2$; CEESO: chlorosulfoxide; CEESO$_2$: chlorosulfone.

All catalysts can be recycled and re-used in further catalytic runs. However, the spent catalysts suffered from the deposition of remarkable amounts of organic deposits, which cannot be removed during the catalytic run even by a careful rising with water or aqueous media (the average amount of the carbon-containing organic deposit, as revealed from TG analysis and C,H,N elemental analysis is around 3.3 - 4.7 wt.%; Figure S16). It was therefore necessary to treat the used catalyst under dry air in a calcination furnace at 500 °C for 1 h, to get rid of the organic deposits.

The performance of Eu-NbSAP in 3 consecutive catalytic cycles was then studied in detail, as this catalyst displayed the highest activity (Figure S17). In the second catalytic run, the catalyst showed a slight decrease in activity and, after 24 h, a maximum conversion of 71% (curve b) was obtained vs. 80 % (Figure S17, curve a). A more enhanced decrease in activity was presented in the third catalytic run (2nd recycle), with lower initial activity and final maximum conversion, 66 % (curve c). The reason for such gradual loss in activity is not fully clear, but it is not likely due to metal leaching, since specific hot-separation tests[30] and analysis of the solid-free filtrate revealed no detectable presence of Nb species.

Optical Detection Tests

The evolution of the main emission band of Eu(III) at 615 nm over time (from *ca.* 10 s up to 3 h) was monitored in aqueous suspensions under continuous stirring. The emission spectrum, under excitation at 395 nm, was recorded both in the absence of CEES and after contact with 100 μL of substrate (286 mM) over time.

The emission spectra of the suspension containing NbEuSAP and CEES at different contact times are shown in Figure 7A. Comparable results were found for Eu-NbSAP (Figure S18). The evolution over time of the band intensity at 615 nm for Eu-NbSAP (a) and NbEuSAP (b) is reported in Figure 7B.

In the absence of the CWA simulant (Figure 7A, black curve (a)), the emission spectra of the Eu-saponites showed the characteristic intra-4f^6 electronic levels of Eu^{3+} ($^5D_0$-^7F_J, J = 0-4)[45] as previously discussed. After addition of 100 μL of CEES, a marked reduction in the intensity of the 615 nm band of Eu^{3+} over time could be clearly observed (Figure 7A): the band started to decrease after few seconds of contact time with the CEES simulant (red curve (b)), and attenuated up to 20% after 3 hours (blue curve (c)). This signal is related to the $^5D_0$-$^7F_2$ electronic transition of europium and it is highly sensitive to changes in local chemical environment around the luminescent sites.[45,53-59] In our study the coordination of CEES molecules to Eu sites could be easily detected. This interaction leads to a drastic and rapid decrease of the emission intensity[41-44]: 16% after 10 s, 34% after 2 min and 71% after 1h of contact time for the NbEuSAP sample (Figure 7B). The same behaviour was observed for Eu-NbSAP: 18% after 10 s, 22% after 2 min and 81% after 1 h of contact with CEES (Figure 7B and Figure S18).

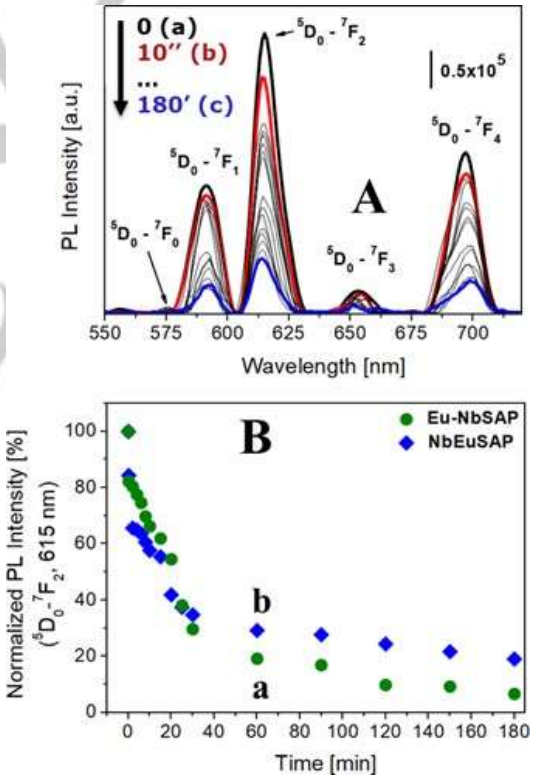

Figure 7. A) Emission spectra of NbEuSAP, under excitation at 395 nm, before (black curve (a)) and after addition of CEES (red curve (b) = 10 s; blue curve (c) = 3 h). The spectra were collected in aqueous suspension, under continuous stirring. B) Normalized PL intensity of the 615 nm band over time for Eu-NbSAP (a) and NbEuSAP (b).

The different behaviour of the two samples, especially within the first minutes may be due to a different accessibility of the Eu^{3+} sites in the two samples containing Eu^{3+} sites with different

location. A possible interaction mechanism between CEES and Eu^{3+} sites in the two cases in reported in Figure S19.
Such results demonstrate both Eu-containing clays have a good detection capability, and we propose that NbEuSAP, featuring the lowest Eu concentration and the best overall luminescence performance, is the most suitable material for the rapid detection of sulfur-containing CWAs.

Conclusions

Two unprecedented bifunctional saponite samples containing europium and niobium in the same material were designed and synthesised. Europium ions were successfully introduced: *i*) in the tetrahedral structural positions together with niobium by a *one-pot* hydrothermal process (NbEuSAP) or *ii*) in the interlayer space of a NbSAP clay through intercalation by ion-exchange procedure (Eu-NbSAP).
In order to approach real use conditions, catalytic tests have been performed under very mild conditions (room temperature, neutral pH and atmospheric pressure) and in the absence of organic solvents (i.e. diluted H_2O_2).
Eu-NbSAP sample was able to degradate ca. 80% of the sulfur mustard agent simulant, CEES, in 6 h because of the synergistic effect of Nb(V) sites and the surface acidity of the clay. The presence of intercalated Eu^{3+} did not therefore significantly inhibit the performance of the catalyst. The sample containing in-framework Eu(III) species (NbEuSAP) decomposed *ca*. 63% of CEES after 24 h in relation of a reduced amount of Nb(V) species inside the framework. In aqueous phase, both solids led to the hydrolysis of the chloroethyl moiety, with the formation of hydroxy-organosulfur by-products.
At the same time, Eu-containing saponite clays were able to detect the presence of CEES rapidly and effectively in aqueous medium, even after few seconds of contact time. The Eu(III) sites in the NbEuSAP material resulted to be more accessible by CEES molecules, thus leading to a more efficient detection of the CWA simulant compared to Eu-NbSAP.
Both solids proved to be potential candidates as bifunctional systems with a detection and catalytic degradation capability for organosulfur chemical warfare agents.

Acknowledgements

The authors gratefully thank Dr. Elena Perin (DiSIT - Università del Piemonte Orientale *"Amedeo Avogadro"*, Alessandria, Italy) for the ICP-AES analyses. The investigation was supported by the Università del Piemonte Orientale (Ricerca locale FAR2019).

Keywords: chemical warfare agent • saponite • lanthanide • abatement • detection • clays

[1] K. Ganesan, S. K. Raza, R. Vijayaraghavan, *J. Pharm. Bioallied. Sci.* **2010**, *2*, 166-178.
[2] G. J. Fitzgerald, *Am. J. Public Health.* **2008**, *98*, 1158.
[3] A. Richardt in *CBRN Protection: Managing the Threat of Chemical, Biological, Radioactive and Nuclear Weapons*, Wiley-VCH, **2012**, ISBN: 978-3-527-32413-2.
[4] R. C. Gupta in *Handbook of Toxicology of Chemical Warfare Agents*, Elsevier Inc., **2015**, ISBN: 978-0-12-800159-2.
[5] A) A. Brunning, *Chemical & Engineering News*, **2015**; B) www.compoundchem.com, retrieved in July 2020.
[6] A) D. R. Coats, *Statement for the Record: 2018 Worlwide Threat Assessment of the US Intelligence Community*, **2019**; B) T. Schneider, T. Lütkefend, *Nowhere to Hide: The Logic of Chemical Weapons Use in Syria*, Global Pulic Policy Institute, **2019**.
[7] *Convention on the Prohibition of the Development, Production, Stockpiling and Use of Chemical Weapons and on their Destruction*, United Nations Treaty Collection, retrieved in July 2020.
[8] C. A. Valdez, R. N. Leif, S. Hok, B. R. Hart*, Reviews in Analytical Chemistry* **2017**, *37***.**
[9] www.opcw.org/about-chemical-weapons/what-is-a-chemical-weapon/, retrieved in July 2020.
[10] F. M. Raushel, *Nature* **2011**, *469*, 310-311.
[11] R. D. Gall, C. L. Hill, J. E. Walker, *Chem. Mater.* **1996**, 8, 2523-2527.
[12] J. R. Soliz, C. J. Karwacki, Pat. US 9770703, B1 20170926, **2017**.
[13] J. R. Hiscock, M. R. Sambrook, N. J. Wells, P. A. Gale, *Chem. Sci.* **2015**, 6, 5680-5684.
[14] R. P. Johnson, C. L. Hill, *Appl. Toxicol.* **1999**, 19(S1), S71-S75.
[15] R. Karthik, J. Vinoth Kumar, S. M. Chen, T. Kokulnathan, H. Y. Yang, V. Muthuraj, *ACS Sustain. Chem. Eng.* **2018**, 6, 7, 8615-8630
[16] A) G. W. Wagner, L. R. Procell, D. C. Sorrick, G. E. Lawson, C. M. Wells, C. M. Reynolds, D. B. Ringelberg, K. L. Foley, G. J. Lumetta, D. L. Blanchard, Jr., *Ind. Eng. Chem. Res.* **2010**, *49*, 3099-3105; B) K. Kim, O. G. Tsay, D. A. Atwood, D. G. Churchill, *Chem. Rev.* **2011**, *111*, 5345-5403.
[17] A) R. D. Albright, *Cleanup of Chemical and Explosive Munitions*, William Andrew, Norwich, **2008**; B) S. Polat, M. Gunata, J. Parlakpinar, *Annals of Medical Research* **2018**, *25*, 776-782; C) E. T. Dickinson, J. S. Love, *J. Emerg. Med. Serv.* **2017**, *2*.
[18] G. K. Prasad, P. V. R. K. Ramacharyulu, B. Singh, K. Batra, A. R. Srivastava, K. Ganesan, R. Vijayaraghavan*., J. Mol. Catal. A: Chemical* **2011**, *349***,** 55-62.
[19] A) Y. C. Yang, J. A. Baker, J. R. Ward, *Chem. Rev.* **1992**, *92*, 1729-1743; B) G. W. Wagner, *Ind. Eng. Chem. Res.* **2011**, *50*, 12285-12287.
[20] A) N. S. Bobbitt, M. L. Mendonca, A. J. Howarth, T. Islamoglu, J. T. Hupp, O. K. Farha, R. Q. Snurr, *Chem. Soc. Rev.* **2017**, *46*, 3357-3385; B) K. Kibong, G. T. Olga, A. A. David, G. C. David, *Chem. Rev.* **2011**, *111*, 5345-5403.
[21] C. Tiozzo, C. Bisio, F. Carniato, M. Guidotti*, Catal. Today* **2014**, *235*, 49-57.
[22] Y. Hou, H. An, S. Chang, J. Zhanga, *Catal. Sci. Technol.* **2019**, *9*, 2445-2455.
[23] N. M. Okun, T. M. Anderson, C. L. Hill, *J. Mol. Catal. A* **2003**, *197*, 283-290.
[24] Ş. Neaţu, Bogdan Cojocaru, V. I. Pârvulescu, V. Şomoghi, M. Alvaro, H. Garcia, *J. Mater. Chem.* **2010**, *20*, 4040-4050.
[25] S. R. Livingston, C. C. Landry, *J. Am. Chem. Soc.* **2008**, *130*, 13214-13215.
[26] Y. Y. Liu, S. Y. Moom, J. T. Hupp, O. K. Farha, *ACS. Nano.* **2015**, *9*, 12358-12364.
[27] I. Timur, A. O. Manuel, P. Emmanuel, J. H. Ashlee, A. V. Nicolaas, A. Ahmet, M. A. Abdullah, J. C. Christopher, K. F. Omar, *Angew. Chem. Int. Ed.* **2018**, *57*, 1-6.
[28] D. T. Lee, J. J. Zhao, G. W. Peterson, G. N. Parsons, *Chem. Mater.* **2017**, *29*, 4894-4903.
[29] Y. Q. Li, Q. Gao, Y. S. Zhou, L. L. Zhang, Y. X. Zhong, Y. Ying, C. Zhang, Y. Q. Liu, Y. A. Wang, *J. Hazard. Mater.* **2018**, *358*,113-121.
[30] F. Carniato, C. Bisio, R. Psaro, L. Marchese, M. Guidotti, *Angew. Chem. Int. Ed.* **2014**, *53*, 10095-10098.
[31] F. Carniato, C. Bisio, C. Evangelisti, R. Psaro, V. Dal Santo, D. Costenaro, L. Marchese, M. Guidotti, *Dalton Trans.* **2018**, *47*, 2939-2948.
[32] F. Carniato, G. Gatti, C. Bisio, *New J. Chem.*, **2020**, *44*, 9969—9980.
[33] M. Burnworth, S. J. Rowan, C. Weder, *Chemistry* **2007**, *13*, 7828-7836.
[34] *Chemical and Biological Terrorism: Research and Development to Improve Civilian Medical Response*, Institute of Medicine (US) Committee on R&D Needs for Improving Civilian Medical Response to Chemical and Biological Terrorism Incidents, Washington (DC): National Academies Press (US), **1999**.
[35] R. Sferopoulos, *A Review of Chemical Warfare Agent (CWA) Detector Technologies and Commercial-Off-The Shelf Items*, Human Protection and Performance Division DSTO Defence Science and

Technology Organisation, 506 Lorimer St Fishermans Bend, Victoria 3207 Australia, **2008**.
[36] E. Dolgin, *Nat. Med.* **2013**, *19*, 1194-1195.
[37] A. Gulland, *Br. Med. J.* **2013**, *347*.
[38] A. Papalardo, M. E. Amato, F. P. Ballistreri, V. L. P. Fragola, G. A. Tomaselli, R. M. Toscano, J. T. Sfrazzetto, *J. Chem. Sci.* **2013**, *125*, 869-873.
[39] E. J. Pacsial-Ong, Z. P. Aguilar, *Frontiers in bioscience (Scholar edition)*, **2013**, *5*, 516-543.
[40] C. M. Whitaker, E. E. Derouin, M. B. O'Connor, C. K. Whitaker, J. A. Whitaker, J. J. Snyder, *J. Macromol. Sci. A* **2016**, *54*, 40-46.
[41] A. J. Metherell, C. Curty, A. Zaugg, S. T. Saad, G. H. Dennison, M. D. Ward, *J. Mater. Chem. C* **2016**, *4*, 9664-9668.
[42] G. H. Dennison, C. Curty, A. J. Metherell, E. Micich, A. Zaugg, M. D. Ward, *RSC Advances* **2019**, *9*, 7615-7619.
[43] G. N. Dennison, C. G. Bochet, C. Curty, J. Ducry, D. J. Nielsen, M. R. Sambrook, A. Zaugg, M. R. Johnston*, Eur. J. Inorg. Chem*. **2016**, *9***,** 1348-1358**.**
[44] G. H. Dennison, M. R. Johnston, *Chem. Eur. J.* **2015**, *21*, 6328-6338.
[45] Y. Wang, N. Lin, *Photochem. Photobiol. Sci.* **2011**, *10*, 42-47.
[46] D. Costenaro, G. Gatti, F. Carniato, G. Paul, C. Bisio, L. Marchese, *Microp. Mesop. Mater.* **2012**, *162*, 159-167.
[47] E. M. Kovacs, E. E. Baradacs, P. Konya, P. Kovacs-Palffy, S. Harangy, E. Kuzmann, J. Konya, N. M. Nagy, *Colloids and Surfaces A: Physicochem. Eng. Aspects* **2017**, 522, 287-294
[48] F. Carniato, C. Bisio, G. Gatti, S. Roncoroni, S. Recchia, L. Marchese, *Catal. Lett.* **2009**, *131*, 42-48.
[49] C. Bisio, G. Gatti, E. Boccaleri, L. Marchese, G.B. Superti H.O. Pastore, M. Thommes, *Microp. Mesop. Mater.*, **2008**, *107*, 90–101.
[50] M. Guidotti, R. Psaro, N. Ravasio, M. Sgobba, F. Carniato, C. Bisio, G. Gatti and L. Marchese, *Green Chem.* **2009**, *11*, 1173-1178.
[51] Kenneth J. Balkus, Jr., Jimin Shi, *Langmuir*, **1996,** *12,* 6277-6281.
[52] J. L. Zatz, C. Yarus, *Pharmaceutical Research* **1986**, *3*, 118-121.
[53] K. Binnemans, C. Gorller-Walrand, *J. Rare Earths* **1996**, *14*, 173-180.
[54] A) S. Marchesi, F. Carniato, E. Boccaleri, *ChemPlusChem*, **2015**, *80*, 915-918. B) A. Beeby, I.M. Clarkson, R.S. Dickins, S. Faulkner, D. Parker, L. Royle, A.S. de Sousa, J.A.G. Williams and M. Woods, *J. Chem. Soc., Perkin Trans.* **1999**, *2*, 493-503.
[55] R. Reisfeld, *Struct. Bonding (Berlin)* **1973**, *13*, 53-98.
[56] S. F. Tang, A. Babai, A. V. Mudring, *Angew. Chem. Int. Ed.* **2008**, *47*, 7631-7638.
[57] P. Zhang, Y. Wang, H. Liu, Y. Chen, *J. Mater. Chem.* **2011**, *21*, 18462-18466.
[58] S. I. Klink, G. A. Hebbink, L. Grave, P. G. B. Oude Alink, F. C. J. M. van Veggel, M. H. V. Werts, *J. Phys. Chem. A*, **2002**, *106*, 3681.
[59] M. H. V. Werts, *Luminescent Lanthanide Complexes, Visible Light Sensitised Red and Near-Infrared Luminescence*, PhD thesis, The Netherlands, **2000**.
[60] R. T. Rewick, M. L. Schumacher, D. L. Haynes, *Appl. Spectrosc.* **1986**, *40*, 152.156.
[61] M. Trejda, B. Pokora, M. Ziolek, *Catal. Today*. **2015**, *254*, 104-110.
[62] A. Gallo, C. Tiozzo, R. Psaro, F. Carniato, M. Guidotti, *J. Catal.* **2013**, *298*, 77-83.
[63] I.D. Ivanchikova, I.Y. Skobelev, N.V. Maksimchuk, E.A. Paukshtis, M.V. Shashkov, O.A. Kholdeeva, *J. Catal.* **2017**, *356*, 85-99.
[64] M. Ziolek, I. Sobczak, P. Decyk, K. Sobanska, P. Pietrzyk, Z. Sojka, *Appl. Catal. B: Env.* **2015**, *164*, 288-296.
[65] J. E. Mondloch, M. J. Katz, W. C. Isley, P. Ghosh, P. Liao, W. Bury, G. W. Wagner, M. G. Hall, J. B. DeCoste, G. W. Peterson, R. Q. Snurr, C. J. Cramer, J. T. Hupp, O. K. Farha, *Nat. Mater.* **2015**, *14*, 512-516.
[66] P. Asha, M. Sinha, S. Mandal, *RSC Adv.* **2017**, *7*, 6691-6696.
[67] W.B. Deichmann, Toxicology of Drugs and Chemicals, New York, Academic Press, Inc., **1969**, 259.

10.1002/chem.202005454

Table of Contents

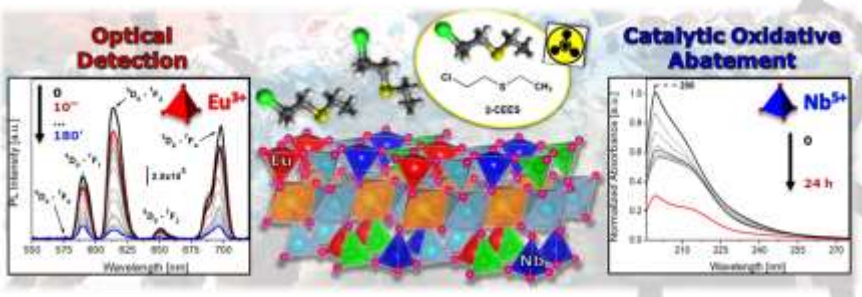

Nb(V)/Eu(III)-containing saponite materials were successfully applied for the first time to the dual optical detection and catalytic oxidative abatement in water, at room temperature of (2-chloroethyl)ethyl sulfide (CEES), a simulant of the blister chemical warfare agent, sulfur mustard.